Femtosecond polarization resolved spectroscopy: A tool for determination of the three-dimensional orientation of electronic transition dipole moments and identification of configurational isomers

Moritz Theisen, Martin Linke, Max Kerbs, Henk Fidder, Mohamed El-Amine Madjet, Angelica Zacarias, and Karsten Heyne

Citation: The Journal of Chemical Physics **131**, 124511 (2009); doi: 10.1063/1.3236804
View online: http://dx.doi.org/10.1063/1.3236804
View Table of Contents: http://scitation.aip.org/content/aip/journal/jcp/131/12?ver=pdfcov
Published by the AIP Publishing

Femtosecond polarization resolved spectroscopy: A tool for determination of the three-dimensional orientation of electronic transition dipole moments and identification of configurational isomers

Moritz Theisen,[1] Martin Linke,[1] Max Kerbs,[2] Henk Fidder,[1] Mohamed El-Amine Madjet,[2] Angelica Zacarias,[1,3] and Karsten Heyne[1,a)]
[1]*Department of Physics, Freie Universität Berlin, Arnimallee 14, 14195 Berlin, Germany*
[2]*Department of Chemistry, Freie Universität Berlin, Fabeckstrasse 36a, 14195 Berlin, Germany*
[3]*European Theoretical Spectroscopy Facility (ETSF)*

(Received 5 May 2009; accepted 3 September 2009; published online 28 September 2009)

A method is presented that combines femtosecond polarization resolved UV/visible pump–IR probe spectroscopy and density functional theory calculations in determining the three-dimensional orientation of an electronic transition dipole moment (tdm) within the molecular structure. The method is demonstrated on the approximately planar molecule coumarin 314 (C314) dissolved in acetonitrile, which can exist in two ground state configurations: the *E*- and the *Z*-isomer. Based on an exhaustive search analysis on polarization resolved measurement data for four different vibrational modes, it is concluded that C314 in acetonitrile is the *E*-isomer. The electronic tdm vector for the electronic $S_0 \rightarrow S_1$ transition is determined and the analysis shows that performing the procedure for four vibrational modes instead of the minimally required three reduces the 1σ probability area from 2.34% to 2.24% of the solution space. Moreover, the fastest rotational correlation time τ_c for the C314 *E*-isomer is determined to be 26 ± 2 ps. © *2009 American Institute of Physics*. [doi:10.1063/1.3236804]

I. INTRODUCTION

Establishment of correlations between molecular structures, temporal changes in structure, and their function in chemical and biophysical reaction mechanisms provides a major challenge in understanding chemistry and biology.[1] Various spectroscopic methods exist for extracting structural information, e.g., x-ray[2] or neutron diffraction,[3] electron microscopy,[4] electron paramagnetic resonance,[5] nuclear magnetic resonance (NMR),[6] Stark spectroscopy,[7] and molecular beam laser spectroscopy.[8] Each of these methods has its own strengths and limitations, and therefore they often provide complementary information. Since the reaction cascade of photoreceptors, for example, spans timescales from femtoseconds to seconds, a complete understanding requires combining several methods capable of yielding structure information on different timescales. NMR, for instance, samples structural dynamics taking place from microseconds to seconds. In recent years much effort has been put in development of femtosecond x-ray diffraction for real-time ultrafast structure determinations. Particularly for biomolecules, radiative damage occurring during these measurements is a serious issue in femtosecond x-ray diffraction,[9] and in view of this the chances are that the outcome may be affected by the interrogating x-ray pulses themselves.

Changes in interactions of water molecules and local structural protein motifs with a protein cofactor in the thermodynamic ground state as well as for reaction intermediates are of utmost importance to understand the reaction mechanisms that natural evolution has optimized.[10] For instance, these interactions can result in structure changes that lead to symmetry breaking. Moreover, the three-dimensional (3D) structure need not be exactly the same *in vivo* as in the gas or crystalline phase. Therefore, it is paramount to develop techniques capable of providing structural information on biological (model) systems in solution phase.[11]

Here we detail an alternative approach for obtaining local structure related information on molecules in solution on femtosecond to nanosecond timescales based on a combination of density functional theory (DFT) calculations and femtosecond polarization resolved UV/visible pump–IR probe spectroscopy. The method makes it possible to determine the 3D orientation of selected electronic transition dipole moments (tdms) of the molecule under investigation. DFT calculations are performed to determine the 3D orientation of vibrational tdms in the electronic ground state. Femtosecond polarization resolved UV/visible pump–IR probe spectroscopy is then used to determine the angle between the electronic tdm of a transition $S_0 \rightarrow S_n$ ($^e\mu_{0\rightarrow n}$) and selected vibrational tdms. For each vibration the angle it makes with the electronic tdm is determined, which therefore defines a cone around the vibrational tdm of all possible orientations the tdm of the pumped electronic transition could have. A unique solution of the full 3D orientation of a selected electronic $^e\mu$ within the molecular frame requires measurement of the angles between at least three linearly independent vibrational tdm vectors and a single selected electronic tdm $^e\mu$. The three cones around the vibrational tdms will intersect in a single unique line that fixes the 3D orientation of the $^e\mu$.

a)Author to whom correspondence should be addressed. Electronic mail: karsten.heyne@fu-berlin.de.

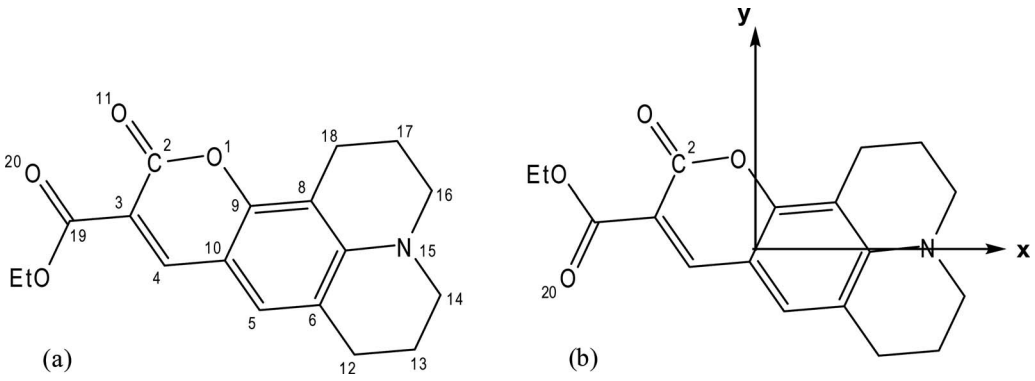

FIG. 1. The two C314 isomeric structures: (a) *Z*-C314 and (b) *E*-C314.

Adding angles with additional vibrational tdms to the analysis potentially reduces the error margins on the determined orientation of the electronic tdm vector, as we will demonstrate.

Precise knowledge of the 3D orientation of electronic tdms within the molecular structure is of particular importance for systems such as photosynthetic complexes, where this orientation serves as an important input parameter for simulations of absorption spectra and energy transfer processes.[12] Recently, we applied the method to determine the 3D orientation of the electronic tdm of the Q_y transition in chlorophyll *a*.[13] Electronic as well as vibrational tdms have frequently been used before to identify molecular conformations and structures. An important advantage of the method presented here is that it does not rely on any technique for preparing macroscopically aligned samples,[14] thereby eliminating uncertainties with respect to the uniqueness of the achieved orientation. In general it is difficult to determine the full orientation distribution function from measuring electronic transitions alone.[15]

Whereas determination of the 3D orientation of an electronic tdm is based on the angles between ground state vibrational bleach signals and an optical excitation induced electronic tdm polarization, dynamic evolution of the polarization of increased absorption signals for vibrational tdms in the electronic excited state contains the potential to reveal information on structural dynamics during the excited electronic state's lifetime. An important aspect is that, in contrast to electronic tdms, many vibrations are associated with rather local structural motifs.

Here the method is used to determine the electronic tdm orientation of the $S_0 \rightarrow S_1$ transition of the laser dye ethyl-2,3,6,7-tetrahydro-11-oxo-1H,5H,-11H[1] benzopyrano [6,7,8-ij]quinolizine-10-carboxylate, also known as coumarin 314 (C314), dissolved in acetonitrile, and as a consequence we implicitly determine its isomeric configuration. C314 is stable upon photoexcitation to the energetically lowest electronic absorption ($S_0 \rightarrow S_1$), which has its maximum at 432 nm. In the midinfrared fingerprint region, C314 exhibits pronounced vibrational absorption bands related to C=O and C=C vibrations. Two stable crystal structures have been identified for C314, one for a yellow colored crystal that corresponds to the *Z*-isomer [*Z*-C314, Fig. 1(a)][16] and another for an orange colored crystal that corresponds to the *E*-isomer [*E*-C314, Fig. 1(b)].[17] The exhaustive search analysis (ExSeA) on the data produces a single consistent solution only for the *E*-isomer, and therefore proves that this is the dominant ground state configurational isomer of C314 dissolved in acetonitrile.

II. MATERIALS AND METHODS

Acetonitrile and C314 were obtained from Sigma-Aldrich and used without further purification. The synthesis of ^{13}C isotopically labeled C314 at position C_3 (C314C) and of ^{13}C isotopically labeled C314 at positions C_2 and C_{19} ($C314C_2$, see Fig. 1) was performed according to the procedure described by Van Gompel and Schuster.[18] The starting materials for these syntheses, 2,3,6,7-tetrahydro-8-hydroxy-1H,5H-benzo[ij]quinolizine-9-carboxaldehyde, diethyl malonate-1, 3-$13C_2$, and diethyl malonate-2-13C, were also obtained from Sigma-Aldrich and used as received.

Polarization resolved femtosecond UV pump/mid-IR probe experiments were performed at room temperature (23 °C) using a Coherent Legend USP Ti:Sa laser/amplifier system. The output of the Coherent Legend USP Ti:Sa laser/amplifier system (pulse duration: 55 fs, wavelength: 800 nm, repetition rate: 1 kHz) was used to generate mid-IR probe pulses in the 5–7 μm spectral range in a three step frequency conversion process and to generate UV pump pulses at 455 nm in a four step frequency conversion process. For the probe pulses, the signal and idler pulses, from a double stage β-barium borate (BBO)-optical parametrical amplifier (type II phase matching, d=4 mm, seeded by white light generated in a sapphire plate), were difference frequency mixed in a $AgGaS_2$ crystal (type I phase matching, d=1 mm). Tunable probe pulses with typical pulse duration of 160 fs, spectral width of 100 cm^{-1}, and 0.6 μJ were obtained. For the pump pulses, idler pulses were generated around 1055 nm from a single stage BBO-optical parametric amplifier (type I phase matching, d=1 mm) pumped at 400 nm, and seeded by white light. These idler pulses were then further amplified in a double stage potassium titanyle arsenate (KTA)-optical parametrical amplifier (type II phase matching, d=5 mm) pumped at 800 nm, yielding pulses with a typical duration of 200 fs, a spectral width of 10 nm, and energy of 130 μJ, which were subsequently sum frequency mixed with 800 nm pulses in a BBO crystal (type I

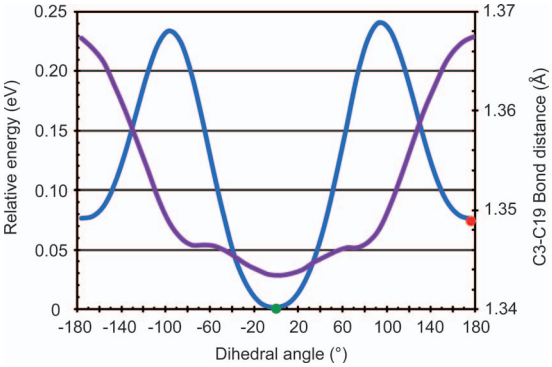

FIG. 2. Dependence of the energy (blue curve) for rotation around the C3–C19 bond. The bond distance change (purple curve) between the C3 and C19 atoms and the bond distances for the isomers *E* (green) and *Z* (red) are also shown. The barrier height for the rotation from the *E*-isomer to the *Z*-isomer is about 0.24 eV.

phase matching, $d=1$ mm) to generate pump pulses at 455 nm, with a spectral width of 270 cm^{-1} and energy of 5 μJ. These pump pulses were attenuated to limit excitation to about 3% of the C314 molecules, far below saturation. The time resolution obtained in the UV pump–IR probe experiment was shorter than 400 fs and mainly limited by group velocity mismatch.

The probe beam is split into two beams with polarizations perpendicular to each other and overlapped with the pump beam within the sample in order to measure simultaneously the signals for both parallel and perpendicular pump-probe polarizations. After passing the sample both probe pulses are dispersed with an imaging spectrograph (grating of 150 lines/mm, $f=320$ mm) and recorded with a 2×32 element mercury-cadmium-telluride (MCT) array detector (resolution of about 1.6 cm^{-1}).

III. RESULTS AND DISCUSSION

A. Ground state calculations on coumarin 314

Based on the work of others,[19–22] we used the 3D molecular structure of the C314 *Z*-isomer, determined experimentally from the crystal structure [Fig. 1(a)], as the starting configuration for DFT calculations with Gaussian code (GAUSSIAN03).[23] Using DFT techniques [hybrid functional B3LYP (Ref. 24) with 6-31G* or 6-31G** basis sets] it was verified that the structures of the *Z*- [Fig. 1(a)] and *E*-isomers [Fig. 1(b)] correspond to local energy minima.[30] Figure 2 shows the relaxed potential energy surface for rotation around the C3–C19 bond. The calculations show that the *E*-isomer is 0.07 eV more stable than the *Z*-isomer. The bond distance between the central atoms used for the calculation of the rotational barrier (C3 and C19) has the shortest distance for the *E*-isomer, suggesting a slightly higher double bond character. Vibrational normal modes and the corresponding tdms were calculated for the optimized structures of the *Z*-isomer and *E*-isomer. The tdm vectors (orange arrows) within the molecular structure of the vibrational modes relevant to the determination of the electronic tdm are shown in Fig. 3. These modes and their tdm vectors $(x/y/z)$ are ν_1(C=C) (−16.658/1.091/−0.856), ν_4(C=C) (19.840/−2.755/0.633), ν_5(C=O) (6.269/11.398/1.241), and ν_6(C=O) (−13.929/20.145/1.751), respectively, for the *E*-isomer. Analogously, for the *Z*-isomer the modes and tdm vectors are ν_1(C=C) (−14.710/0.610/−0.678), ν_4(C=C) (21.601/−3.207/0.508), ν_5(C=O) (−8.123/1.950/−0.920), and ν_6(C=O) (−17.679/20.717/1.437), respectively. The significant difference in the tdm vectors for the ν_5(C=O) mode creates the possibility of distinguishing the *E*-isomer [Fig. 3(e)] and *Z*-isomer [Fig. 3(g)] in our experiments.

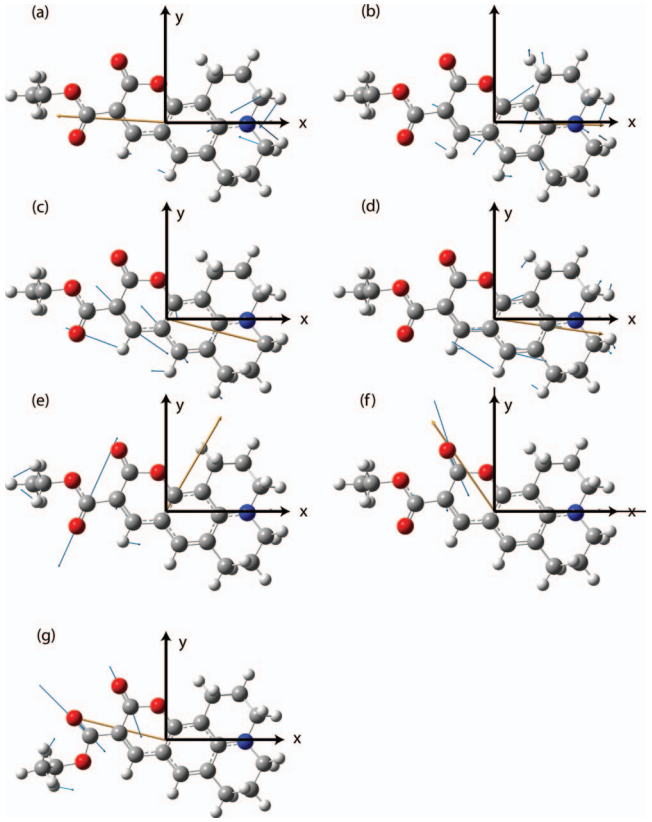

FIG. 3. Calculated IR vibrations and tdms with atomic displacements (blue arrows) and the tdm orientations (orange arrows) for the [(a)–(f)] υ_1(C=C), υ_2(C=C), υ_3(C=C), υ_4(C=C), υ_5(C=O), and υ_6(C=O) vibrations of *E*-C314 and for the (g) υ_5(C=O) vibration of *Z*-C314. Note that the vibrational tdm fixes an orientation but not a direction.

B. Assignment of the vibrational spectrum

Steady-state vibrational absorption spectra of C314 and the isotopically labeled C314C and $C314C_2$, dissolved in acetonitrile, after subtraction of solvent contributions, are presented in Fig. 4. In the spectral range from 1500 to 1800 cm^{-1} six distinct absorption bands are visible that are assigned to four vibrational modes with C=C stretching character and two C=O stretching modes (see Table I).

Upon ^{13}C labeling at position C_3 (C314C) the ν_1(C=C), ν_2(C=C), and ν_3(C=C) vibrations shift by −3, −3, and −6 cm^{-1}, respectively, in agreement with calculated shifts of −2, −4, and −10 cm^{-1}, respectively. Double ^{13}C labeling of the carbon atoms of the two carbonyl groups at positions C_2 and C_{19} ($C314C_2$) result in significant shifts of the ν_5(C=O) and ν_6(C=O) vibrations to lower energies of −38 and −43 cm^{-1}, respectively, in line with calculated shifts of −41/−43 and −44/−45 cm^{-1}. Shifts of the other four vibrations are negligible. Calculated isotopic shifts for

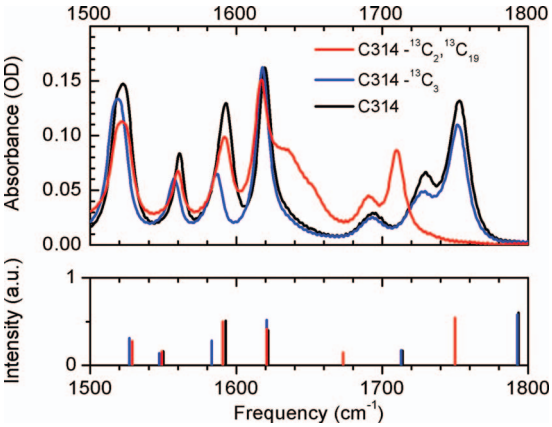

FIG. 4. Upper panel: Steady-state vibrational absorption spectrum of coumarin 314 (black line), $^{13}C_3$-coumarin 314 (blue line), and $^{13}C_2$, $^{13}C_{19}$-coumarin 314 (red line) in acetonitrile, for the region relevant to the femtosecond polarization resolved experiments. Lower panel: Calculated vibrational absorption bands in vacuum of these three coumarin 314 isotopes (scaled by 0.97).

the *E*- and *Z*-isomers of C314C or $C314C_2$ show negligible differences for these modes between the two isomers. Therefore, the two C314 configurational isomers cannot be distinguished by comparing the experimentally observed isotope shifts for these vibrations. However, this question can be solved with our method by comparing the additional structural information on the vibrational tdm orientations for the calculated structures.

C. Calculation of the electronic transition dipole moment

For the full geometry reoptimization we used DFT with the B3LYP exchange-correlation functional and a 6-31G** basis set as implemented in the program JAGUAR.[25] Electronic structure calculations were carried out with the Q-CHEM software package[26] based on the fully optimized geometry. The excitation energies and tdms to the first ten excited states were calculated using time-dependent DFT with the standard B3LYP exchange-correlation functional. Permanent and transition dipole moments were calculated with Q-CHEM using the ground state and transition state electron densities, respectively.

The ground state permanent dipole moment vector (μ_0) was calculated to be $\mu_{0,E}=(\mu_x,\mu_y,\mu_z)=(7.2999,-2.9577,-0.1494)$ for *E*-C314 and $\mu_{0,Z}=(8.0609,-5.8957,-0.1377)$ for *Z*-C314. Calculations of the electronic tdms result in a $S_0\rightarrow S_1$ electronic tdm of ${}^e\mu_{0\rightarrow 1,E}=(-3.1347,0.5917,-0.0950)$ for *E*-C314 and ${}^e\mu_{0\rightarrow 1,Z}=(-3.1502,0.4454,-0.0521)$ for *Z*-C314, both spectrally well separated from other significant transitions. The angles between the calculated ground state permanent dipole moment vector μ_0 and the calculated tdm vector ${}^e\mu_{0\rightarrow 1}$ are $-13°$ and $-28°$ for the *E*-C314 and *Z*-C314, respectively, contrasting with the statement of Benderskii and Eisenthal[19] that they are oriented parallel.

D. Femtosecond polarization resolved UV pump–IR probe experiments

The polarization resolved transient vibrational absorption dynamics of C314 after $S_0\rightarrow S_1$ excitation can reflect the fluorescence lifetime τ_f of the electronic excited state, the rotational anisotropy decay, and in case of efficient internal conversion relaxation of a vibrationally hot electronic ground state. For C314 the latter is a negligible process. In general a molecule has three different moments of inertia and at most five rotational correlation times τ_c.[27] In our experiments only the shortest rotational correlation time τ_c could be determined within the experimental time window of 100 ps. Transient signals of selected bleaching bands are presented for isotropic conditions in Fig. 5(a) and for parallel and perpendicular pump-probe polarizations in Fig. 5(b). The isotropic response was constructed by adding the signal for parallel polarization and twice the signal for perpendicular polarization. The decay of the isotropic signals is governed by the fluorescence lifetime τ_f only, which lies in the nanosecond regime,[20] and therefore causes negligible decay during the first 100 ps. For parallel and perpendicular polarized transients an additional much shorter time constant is observed of 26 ± 2 ps, in line with experiments on a similar molecule coumarin 153.[28] This rotational correlation time τ_c is associated with the smallest moment of inertia, with its axis of revolution roughly parallel to the *x*-axis in Fig. 1. Assuming for now that the effect of rotation around the other two rotational axes is negligible, there are three conditions under which rotation around a single axis has no effect on the anisotropy of the transient IR vibrational absorption signals: (1) if the vibrational tdm vector is parallel to the rotational axis, (2) if the vibrational tdm vector makes an angle of 54.7°

TABLE I. Comparison of the measured and calculated frequencies in cm^{-1}. Calculated frequencies are scaled with a factor of 0.97.

	ν_1(C=C)	ν_2(C=C)	ν_3(C=C)	ν_4(C=C)	ν_5(C=O)	ν_6(C=O)
C314 (measured)	1522	1562	1592	1622	1729	1753
E-C314	1528	1550	1593	1622	1714	1794
Z-C314	1529	1550	1596	1622	1739	1812
C314C (measured)	1519	1559	1586	1621	1728	1752
E-C314C	1526	1546	1583	1621	1713	1793
Z-C314C	1527	1546	1586	1621	1738	1811
$C314C_2$ (measured)	1522	1561	1591	1619	1691	1710
E-$C314C_2$	1528	1548	1591	1622	1673	1750
Z-$C314C_2$	1529	1548	1596	1622	1696	1767

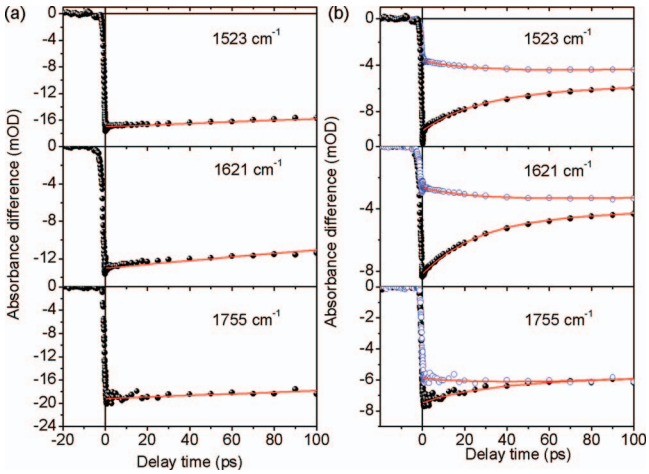

FIG. 5. Transients (symbols) and fitted curves (solid line). (a) Transients of the isotropic signals ($A_{iso}=A_{par}+2A_{perp}$) of C314 for various frequencies. (b) Transients at various frequencies for probe polarizations parallel (solid circles) and perpendicular (open circles) to the pump pulse polarization.

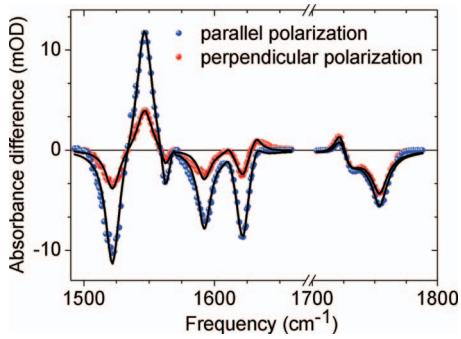

FIG. 6. DASs at time zero for probe pulse polarizations parallel (blue circles) and perpendicular (red circles) to the pump pulse. Solid lines: Simulations of the two DASs with six Lorentzian lineshapes for the ground state and excited state, respectively.

(magic angle) with the electronic tdm, or (3) if the electronic tdm vector is parallel to the rotational axis. In the latter case for each individual vibration the vibrational tdm vectors of the ensemble of molecules are isotropically distributed on a cone around the electronic tdm (and axis of rotation), with opening angle determined by the intramolecular angle between the vibrational and electronic tdms. In Fig. 5(b) the transients and fits for parallel and perpendicular polarizations are plotted for selected vibrational bands. After 100 ps the transients at 1755 cm^{-1}, corresponding to the ν_6(C=O) vibration, exhibit no residual anisotropy, i.e., the signals for parallel and perpendicular polarizations are identical, while for transients at 1523 cm^{-1} [ν_1(C=C)] and 1621 cm^{-1} [ν_4(C=C)] a residual anisotropy remains [Fig. 5(b)]. Due to the decaying anisotropy we can conclude that the electronic tdm vector is not parallel to the axis of rotation for the smallest moment of inertia. The small anisotropy amplitude for the transient at 1755 cm^{-1} indicates a cone angle of this vibrational tdm to the electronic tdm close to the magic angle. After a longer time, when all rotation correlation times[20,21] have affected the signal, all anisotropic contributions will decay.

The total decay associated spectrum (DAS), i.e., the initial signals at $t=0$ ps, were obtained for both polarizations by extrapolating to $t=0$ ps the fits obtained from a global fitting procedure that yielded two exponential decay components of 26 ps and 1.4 ns, respectively. To determine the pure bleaching amplitudes without the impact of overlapping positive signals, the perturbed free induction decays at negative delay times were fitted for pronounced bleaching bands to extract the amplitudes at $t=0$ ps for both polarizations. The isotropic negative signals extrapolated to $t=0$ ps correspond to the steady-state vibrational absorption. These are needed for decomposing the DAS in the negative and positive signal contributions, of which the results are shown in Fig. 6.

E. Analysis of the data

The DASs in Fig. 6 were reconstructed for both polarizations with six Lorentzian vibrational absorption bands for the electronic ground state and six Lorentzian absorption bands for the electronic excited state. The spectral positions and Lorentzian widths of the bleaching bands were determined by steady-state IR absorption spectroscopy, and these parameters were fixed in the fitting procedure. The outcome of the optimal fit of the DAS was used to evaluate the dichroic ratios D of the vibrational modes ($D=A_{\parallel}/A_{\perp}$, with $A_{\parallel}$ and $A_{\perp}$ the absorption changes for parallel and perpendicular polarizations, respectively). The resulting relative angles Θ ($\Theta=\arccos[(2D-1)/(D+2)]^{1/2}$) with 1σ error ranges calculated with the standard $\pm$error margins are presented in Table II. This method does not take the full multidimensional solution space into account.[29]

If the values give unphysical results, the too optimistic error margins of the standard procedure prevent obtaining a physical solution within the 1σ error range of the multidimensional solution surface, and therefore the angle is con-

TABLE II. Relative angles measured between the electronic tdm and vibrational tdms for the ground state and excited state. 1σ standard error margins are in parentheses.

Vibration	State	Frequency (cm^{-1})	Angle (deg)	State	Frequency (cm^{-1})	Angle (deg)
ν_1(C=C)	S_0	1522	6 (+1/−2)	S_1	1546	0 (+4/⋯)
ν_2(C=C)	S_0	1562	15 (+1/−2)	S_1	1568	⋯
ν_3(C=C)	S_0	1592	15 (+1/−1)	S_1	1611	36 (+2/−1)
ν_4(C=C)	S_0	1622	⋯	S_1	1632	51 (+2/−1)
ν_5(C=O)	S_0	1729	60.5 (+0.4/−0.3)	S_1	1723	63.4 (+0.3/−0.3)
ν_6(C=O)	S_0	1753	45.8 (+0.2/−0.1)	S_1	1750	46 (+2/−1)

TABLE III. Relative angles measured between the electronic tdm and vibrational tdms for the ground state and excited state. ExSeA 1σ error margins are in parentheses.

Vibration	State	Frequency (cm^{-1})	Angle (deg)	State	Frequency (cm^{-1})	Angle (deg)
ν_1(C=C)	S_0	1522	6 (+17/−6)	S_1	1546	0 (+19/⋯)
ν_2(C=C)	S_0	1562	15 (+22/−15)	S_1	1568	18 (+72/−18)
ν_3(C=C)	S_0	1592	15 (+7/−15)	S_1	1617	36 (+54/−36)
ν_4(C=C)	S_0	1622	6 (+15/−6)	S_1	1636	51 (+39/−51)
ν_5(C=O)	S_0	1729	61 (+14/−12)	S_1	1723	63 (+12/−10)
ν_6(C=O)	S_0	1753	46 (+10/−11)	S_1	1750	46 (+44/−46)

sidered undeterminable. Consequently, we also applied ExSeA (Ref. 29) to obtain a more reasonable mapping of the error range. Results for the angles and their 1σ ranges are presented in Table III.

The multidimensionality of the solution space is taken into account in the ExSeA and allows determination of all angle ranges with larger but more realistic error margins. The angles with the highest accuracy are those for ν_1, ν_4, ν_5, and ν_6. The angles indicate that the possible solutions for the electronic tdm vector lie on a cone with the determined (opening) angle for a given vibration. We now select first the cones around ν_1, ν_4, and ν_6 and determine their intersection. For three or more noncoplanar vibrational tdm orientations only one intersection of the cones should exist, which is identified as the orientation of the electronic tdm.[13] Since we do not consider a single value of the angle for each cone but explicitly consider the probability distribution around the most probable value, a range of three-cone-intersections with associated probabilities is obtained.

The probability of a specific angle Θ for a single cone distribution can be determined by the ExSeA, which provides an angle range for a given confidence level. For every angle Θ the highest confidence level $c_{\max}$ with angle range containing the angle Θ was determined to weight the probability by $(1-c_{\max})/100$. For example, if a specific angle Θ lies in the angle range of the confidence level of $c_{\max}=70\%$ but not of $c=69.9\%$, the assigned probability is 0.3. After assigning all angle probabilities, they are normalized. With this procedure we are able to assign a probability P to each cone angle Θ and determine the asymmetric error ranges. The intersection for three or more cone angles fixes the orientation of the electronic tdm.[13]

Without any additional requirements the 3D orientation of ${}^e\mu_{0\to1}$ within the molecular frame can be obtained by solving the linear equation

$$\begin{pmatrix} \mu_{1,x} & \mu_{1,y} & \mu_{1,z} \\ \mu_{2,x} & \mu_{2,y} & \mu_{2,z} \\ \mu_{3,x} & \mu_{3,y} & \mu_{3,z} \end{pmatrix} \begin{pmatrix} {}^e\mu_x \\ {}^e\mu_y \\ {}^e\mu_z \end{pmatrix} = \begin{pmatrix} \cos\Theta_1 \\ \cos\Theta_2 \\ \cos\Theta_3 \end{pmatrix},$$

where the matrix contains the calculated orientations of the vibrational tdm vectors and Θ_i are the three measured angles. Note that two solutions are associated with each cosine Θ_i term. The vector solution of this equation is the intersection of the three cones. The variation of the measured angles Θ_i gives a distribution of solutions $\Theta_{i,j}$, where j denotes the discrete solutions for the measured angle Θ_i. The probability of a specific solution for three measured angles is given by

$$P({}^e\mu) = \frac{P(\Theta_1)P(\Theta_2)P(\Theta_3)}{\Sigma_{i,j,k}(P(\Theta_{1,i})P(\Theta_{2,j})P(\Theta_{3,k}))},$$

where the denominator represents the normalization factor. As a result we receive a 3D solution surface, color coded for different probability ranges [Fig. 8]. From the solution space we can determine the orientation of the electronic tdm, which is given by $(x/y/z)=(-0.987/0.159/-0.029)$. The solution space of the electronic tdm unit vector is plotted in Fig. 7 as projections on different Cartesian planes. Although the error margins according to Fig. 8 seem symmetric around the optimal solution on the 3D sphere, it is clear from Fig. 7 that the error margins can become very asymmetric for projections on different Cartesian planes. For a multidimensional asymmetric probability distribution it is ambiguous to define a one-dimensional 1σ range for a Cartesian coordinate. However, a multidimensional 68% probability range can be determined. Since we have a continuous solution space, we can integrate along decreasing probabilities until we reach an integrated probability of 0.6827. The integration limit defines the level curve of the P_σ range. The resulting 3D P_σ range presented in Fig. 8 (green color) can be com-

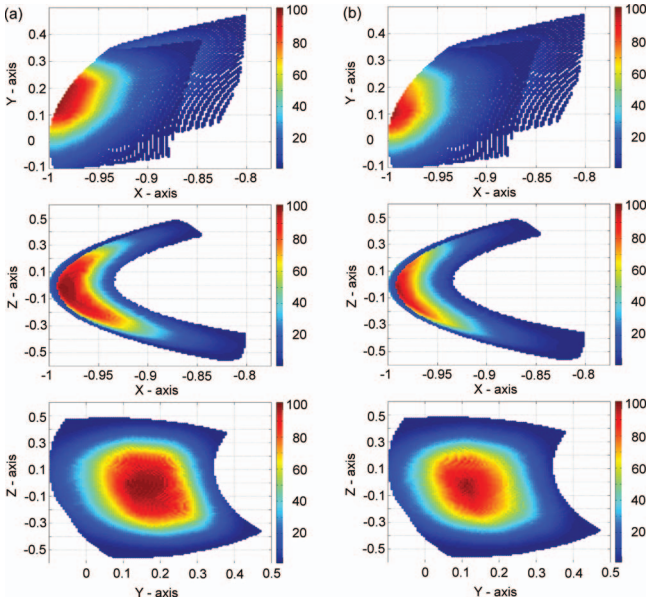

FIG. 7. Projections of the 3D solution on the Cartesian planes using (a) the three vibrational tdms ν_1(C=C), ν_4(C=C), and ν_6(C=O) and (b) the four vibrational tdms ν_1(C=C), ν_4(C=C), ν_5(C=O), and ν_6(C=O).

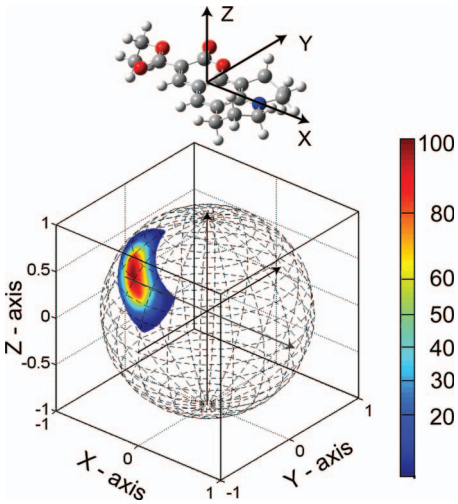

FIG. 8. 3D solution surface of the $S_0 \rightarrow S_1$ electronic tdm of C314. The color indicates the relative probability of a specific direction for the tdm. The solution surface is located on the surface of the unit sphere (dashed) with an optimal solution at ${}^{e}\mu_{0\rightarrow 1}=(-0.994/0.107/-0.020)$. Note that the second and opposite solution $-({}^{e}\mu_{0\rightarrow 1})$ is not shown.

pared with the entire surface of the half-sphere to estimate the precision of the result. Here, the 3D P_{σ} range covers 2.34% of the half-sphere surface, while the 3D $P_{2\sigma}$ range covers 7.17%.

The method presented here intrinsically combines experimental data with results from theoretical DFT calculations in order to extract the electronic tdm vector. Therefore, next to experimental error margins, uncertainties in the calculated vibrational tdm vectors for the electronic ground state may affect the accuracy of the final result. If the actual vibrational tdm vectors deviate in a correlated manner from the calculated vectors (all rotated over the same space angle) this will result in an inaccessible systematic error. This situation is, however, highly unlikely for the (minimally) three linearly independent vibrational tdms required to perform the analysis. If deviations between calculated and actual vibrational tdms are uncorrelated, using an increased number of vibrational tdms should average out the influence of these deviations on the end result. The planarity of C314 should make this molecule fairly rigid to changes in solvent polarity. Uncertainties in the vibrational tdm vectors determined with DFT calculations are therefore expected to be considerably smaller than the 1σ error ranges for the experimental data listed in Table III, and as a consequence exert an immaterial influence on the obtained electronic tdm vector.

A higher precision is obtained by using more than three vibrational tdms. Introducing a fourth cone angle of the vibrational υ_5(C=O) mode, we get a narrower probability distribution, which results in an electronic tdm orientation of $(x/y/z)=(-0.994/0.107/-0.020)$. It is obvious from Fig. 7(b) that the solution calculated with four vibrational tdms has a higher precision. This is also reflected in the 3D P_{σ} range, which becomes narrower and covers now 2.24% of the half-sphere. As seen in Fig. 7, the error margin for the determined electronic tdm vector is twice as big for the projection on the z-axis as for the projection on the y-axis. The smallest error margin is found for the projection on the x-axis. The largest error margin for the z-axis component is to be expected, since the used vibrational tdms have only small z-components. Assuming a symmetrical distribution the 1σ probability surface area of 2.24% would correspond to a space angle of about $\pm 8°$. Improving the signal to noise ratio of the data and selecting vibrational tdms with significant contributions in all directions can further enhance the precision of the result.[13] Furthermore, the electronic tdm vector determined with four vibrations makes an angle of 4.6° with the theoretically calculated tdm vector for the E-isomer of C314, indicating that within the error margins experiment and theory are in agreement. Note that the angle between the theoretically determined ${}^{e}\mu_{0\rightarrow 1,E}$ and ${}^{e}\mu_{0\rightarrow 1,Z}$ is only 2.8°.

The intersections of the 1σ cones of vibrations ν_1, ν_4, and ν_6 are presented in Fig. 7(a) for the C314 E-isomer. A similar solution is obtained for the C314 Z-isomer. Introducing a fourth cone angle of the vibrational υ_5(C=O) mode there is no intersection of these three cones with that of the ν_5 vibration for the Z-isomer. In contrast, we do obtain a single solution for all investigated vibrations for the E-isomer [Figs. 7(b) and 8], and as a consequence the unique orientation of the $S_0 \rightarrow S_1$ electronic tdm ${}^{e}\mu_{0\rightarrow 1,E}$ for the C314 molecule. The ability to distinguish between the E- and Z-isomer therefore is solely due to the markedly different vibrational tdm orientations of ν_5(C=O) in these two isomers [see Figs. 3(e) and 3(g)], and the experimental data indicate that our compound in actonitrile is predominantly the E-isomer of C314. This is in line with the conclusion from the gas-phase DFT calculations that the E-isomer is 0.07 eV more stable than the Z-isomer. If a similar energy difference persists in acetonitrile solutions of C314 maximally 7% of C314 would be the Z-isomer in thermodynamic equilibrium.

IV. CONCLUSIONS

A new method was detailed that allows the determination of an electronic tdm orientation within the molecular structure. This method combined polarization resolved femtosecond UV/visible pump–IR probe spectroscopy, ExSeA on the experimental data, and DFT calculations in the electronic ground state. DFT calculations provided the ground state vibrational tdm vectors of the C=C stretching and C=O stretching vibrations selected for experimental investigation. Femtosecond polarization resolved visible pump–IR probe experiments then allowed the determination of the angles these vectors make with the electronic tdm ${}^{e}\mu_{0\rightarrow 1}$ of the $S_0 \rightarrow S_1$ transition, selected through optical excitation. Combining cones of the orientation distribution given by these determined (opening) angles results in a unique intersection only for the C314 E-isomer. Consequently, the C314 Z-isomer can be ruled out as the (dominant) isomer of C314 in acetonitrile solution at room temperature. In agreement with this, gas-phase DFT calculations for the rotational barrier around the isomerization bond demonstrated that the E-isomer is expected to be 0.07 eV more stable than the Z-isomer. The electronic tdm orientation for the $S_0 \rightarrow S_1$ transition, determined with experimental angle data for four different vibrations, is $(x/y/z)=(-0.994/0.107/-0.020)$, with

the reduced 1σ probability covering 2.24% of the half-sphere solution surface, whereas the reduced 1σ probability covered 2.34% of the solution surface if only three vibrations were used to determine the orientation. The experimentally determined electronic tdm vector deviates only 4.6° from the orientation calculated theoretically with Q-CHEM. From polarization resolved femtosecond visible pump–IR probe measurements it is further concluded that the fastest rotational correlation time of the C314 *E*-isomer is 26 ± 2 ps.

ACKNOWLEDGMENTS

We appreciate the support from the Deutsche Forschungsgemeinschaft (SFB 498), the EU 7th Framework Program through the ETSF Integrated Infrastructure Initiative (I3 Grant No. 211956), and the FUB Computing Center (ZEDAT).

[1] R. Y. Tsien, Annu. Rev. Biochem. **67**, 509 (1998); J. W. Peters, W. N. Lanzilotta, B. J. Lemon, and L. C. Seefeldt, Science **282**, 1853 (1998); V. Sundström, T. Pullerits, and R. van Grondelle, J. Phys. Chem. B **103**, 2327 (1999).
[2] F. Schotte, M. H. Lim, T. A. Jackson, A. V. Smirnov, J. Soman, J. S. Olson, G. N. Phillips, M. Wulff, and P. A. Anfinrud, Science **300**, 1944 (2003).
[3] D. I. Svergun, S. Richard, M. H. J. Koch, Z. Sayers, S. Kuprin, and G. Zaccai, Proc. Natl. Acad. Sci. U.S.A. **95**, 2267 (1998).
[4] W. Kühlbrandt, D. N. Wang, and Y. Fujiyoshi, Nature (London) **367**, 614 (1994).
[5] R. Bittl, S. G. Zech, P. Fromme, H. T. Witt, and W. Lubitz, Biochemistry **36**, 12001 (1997).
[6] P. Düx, G. Rubinstenn, G. W. Vuister, R. Boelens, F. A. A. Mulder, K. Hard, W. D. Hoff, A. R. Kroon, W. Crielaard, K. J. Hellingwerf, and R. Kaptein, Biochemistry **37**, 12689 (1998).
[7] I. T. Suydam, C. D. Snow, V. S. Pande, and S. G. Boxer, Science **313**, 200 (2006); S. G. Boxer, J. Phys. Chem. B **113**, 2972 (2009); D. A. Mitchell, P. J. Morgan, and D. W. Pratt, J. Phys. Chem. A **112**, 12597 (2008).
[8] E. Nir, K. Kleinermanns, and M. S. de Vries, Nature (London) **408**, 949 (2000); J. R. Johnson, K. D. Jordan, D. F. Plusquellic, and D. W. Pratt, J. Chem. Phys. **93**, 2258 (1990); W. E. Sinclair and D. W. Pratt, *ibid.* **105**, 7942 (1996).
[9] R. Neutze, R. Wouts, D. van der Spoel, E. Weckert, and J. Hajdu, Nature (London) **406**, 752 (2000).
[10] M. A. Steffen, K. Q. Lao, and S. G. Boxer, Science **264**, 810 (1994); L. Song, M. A. El-Sayed, and J. K. Lanyi, *ibid.* **261**, 891 (1993); G. Bublitz, B. A. King, and S. G. Boxer, J. Am. Chem. Soc. **120**, 9370 (1998).
[11] I. B. Klenina, I. V. Borovykh, A. Y. Shkuropatov, P. Gast, and I. I. Proskuryakov, Chem. Phys. **294**, 451 (2003); M. Lim, T. A. Jackson, and P. A. Anfinrud, Science **269**, 962 (1995); D. von Stetten, M. Günther, P. Scheerer, D. H. Murgida, M. A. Mroginski, N. Krauß, T. Lamparter, J. Zhang, D. M. Anstrom, R. D. Vierstra, K. T. Forest, and P. Hildebrandt, Angew. Chem., Int. Ed. **47**, 4753 (2008); P. Hamm, M. Lim, W. F. DeGrado, and R. M. Hochstrasser, Proc. Natl. Acad. Sci. U.S.A. **96**, 2036 (1999); P. Hamm, M. H. Lim, and R. M. Hochstrasser, J. Phys. Chem. B **102**, 6123 (1998).
[12] F. Müh, T. Renger, and A. Zouni, Plant Physiol. Biochem. **46**, 238 (2008); G. Raszewski and T. Renger, J. Am. Chem. Soc. **130**, 4431 (2008); B. A. King, A. de Winter, T. B. McAnaney, and S. G. Boxer, J. Phys. Chem. B **105**, 1856 (2001); A. R. Holzwarth, M. G. Müller, J. Niklas, and W. Lubitz, Biophys. J. **90**, 552 (2006).
[13] M. Linke, A. Lauer, T. von Haimberger, A. Zacarias, and K. Heyne, J. Am. Chem. Soc. **130**, 14904 (2008).
[14] M. Fragata, B. Nordén, and T. Kurucsev, Photochem. Photobiol. **47**, 133 (1988); M. A. M. J. van Zandvoort, D. Wrobel, P. Lettinga, G. van Ginkel, and Y. K. Levine, *ibid.* **62**, 299 (1995).
[15] J. Michl and E. W. Thulstrup, *Spectroscopy with Polarized Light* (VCH, New York, 1986); M. A. M. J. van Zandvoort, H. C. Gerritsen, G. van Ginkel, Y. K. Levine, R. Tarroni, and C. Zannoni, J. Phys. Chem. B **101**, 4149 (1997).
[16] B. C. Yip, H. K. Fun, K. Sivakumar, Z. Y. Zhou, O. B. Shawkataly, and S. G. Teoh, Acta Crystallogr., Sect. C: Cryst. Struct. Commun. **51**, 956 (1995).
[17] T. Honda, I. Fujii, N. Hirayama, N. Aoyama, and A. Miike, Acta Crystallogr., Sect. C: Cryst. Struct. Commun. **52**, 395 (1996).
[18] J. Van Gompel and G. B. Schuster, J. Org. Chem. **52**, 1465 (1987).
[19] A. V. Benderskii and K. B. Eisenthal, J. Phys. Chem. B **105**, 6698 (2001).
[20] D. Zimdars, J. I. Dadap, K. B. Eisenthal, and T. F. Heinz, J. Phys. Chem. B **103**, 3425 (1999).
[21] K. T. Nguyen, X. M. Shang, and K. B. Eisenthal, J. Phys. Chem. B **110**, 19788 (2006).
[22] R. S. Koefod and K. R. Mann, Inorg. Chem. **30**, 2221 (1991).
[23] M. J. Frisch G. W. Trucks, H. B. Schlegel *et al.*, GAUSSIAN 03, Revision B.04, Gaussian, Inc., Pittsburgh, PA, 2003.
[24] C. T. Lee, W. T. Yang, and R. G. Parr, Phys. Rev. B **37**, 785 (1988); A. D. Becke, J. Chem. Phys. **98**, 5648 (1993); B. Miehlich, A. Savin, H. Stoll, and H. Preuss, Chem. Phys. Lett. **157**, 200 (1989).
[25] L. L. C. Portland, JAGUAR 5.5, Schrödinger, OR, 1991–2003.
[26] J. Kong, C. A. White, A. I. Krylov, D. Sherrill, R. D. Adamson, T. R. Furlani, M. S. Lee, A. M. Lee, S. R. Gwaltney, T. R. Adams, C. Ochsenfeld, A. T. B. Gilbert, G. S. Kedziora, V. A. Rassolov, D. R. Maurice, N. Nair, Y. H. Shao, N. A. Besley, P. E. Maslen, J. P. Dombroski, H. Daschel, W. M. Zhang, P. P. Korambath, J. Baker, E. F. C. Byrd, T. Van Voorhis, M. Oumi, S. Hirata, C. P. Hsu, N. Ishikawa, J. Florian, A. Warshel, B. G. Johnson, P. M. W. Gill, M. Head-Gordon, and J. A. Pople, J. Comput. Chem. **21**, 1532 (2000).
[27] T. J. Chuang and K. B. Eisenthal, J. Chem. Phys. **57**, 5094 (1972); M. Ehrenberg and R. Rigler, Chem. Phys. Lett. **14**, 539 (1972).
[28] M. L. Horng, J. A. Gardecki, and M. Maroncelli, J. Phys. Chem. A **101**, 1030 (1997).
[29] T. A. Roelofs, C. H. Lee, and A. R. Holzwarth, Biophys. J. **61**, 1147 (1992).
[30] See EPAPS supplementary material at http://dx.doi.org/10.1063/1.3236804 for atomic coordinates of the C314 E- and Z-isomer molecular structures, and anisotropy signals.